coordinate estimated, to a first-order approximation, by Cruickshank & McDonald (1967) in the case of least-squares refinement. The same kind of considerations reported by these authors on the vanishing of the coordinate errors when the reflexions are collected according to a tetrahedral arrangement of the spherical octants, also applies to the present case.

Use of $|F_0(\mathbf{H})|$ and $\alpha^0(\mathbf{H})$

If we carry out an electron density computation using, in a relation like (19), phases $\alpha^0(\mathbf{H})$ [or $\alpha^r(\mathbf{H})$] and $|F_o(\mathbf{H})|$ it may be deduced, on the basis of Ramachandran's β synthesis (Ramachandran, 1964), that the map will show maxima in the correct $\mathbf{r}_j$ positions but they are incorrect in shape and weight. Further, there are also satellite maxima, whose weights depend on the $\Delta f''$ values, in positions defined by combinations of interatomic vectors.

To a first order approximation we can write

$$|F_o(\mathbf{H})| \exp [i\alpha^0(\mathbf{H})] = \frac{|F_o(\mathbf{H})| \cdot |F^0(\mathbf{H})|}{|F^0(\mathbf{H})|} \exp [i\alpha^0(\mathbf{H})]$$

$$\simeq \frac{|F_o(\mathbf{H})|^2}{|F^0(\mathbf{H})|} \exp [i\alpha^0(\mathbf{H})] . \quad (29)$$

If we assume that there are P and Q atoms in the unit cell having f^0 (or f^r) and $\Delta f''$ scattering factors respec-

tively (the Q atoms being in the same positions as the P atoms), the analogy with the β synthesis is evident by putting, according to the notation of Ramachandran,

$$F_o(\mathbf{H}) \rightarrow F_N \text{ and } F^0(\mathbf{H}) \rightarrow F_P \quad (30)$$

where $N = P + Q$.

Consequently, it must be noted that the same atoms, with the same $\Delta f''$ values, when packed in different structures, give rise to different spurious peaks and errors. Furthermore, there is, at present, no direct comparison between the magnitudes of these errors and of those described in the $|F_o(\mathbf{H})|$ and $\alpha(\mathbf{H})$ case.

References

CRUICKSHANK, D. W. J. & McDONALD, W. S. (1967). Acta Cryst. 23, 9.
FERRARIS, G. (1969). Acta Cryst. B25, 1544.
IBERS, J. A. & HAMILTON, W. C. (1964). Acta Cryst. 17, 781.
JAMES, R. W. (1950). The Optical Principles of the Diffraction of X-rays, p. 138. London: Bell.
McDONALD, W. S. & CRUICKSHANK, D. W. J. (1967). Acta Cryst. 22, 48.
PATTERSON, A. L. (1963). Acta Cryst. 16, 1255.
RAMACHANDRAN, G. N. (1964). Advanced Methods of Crystallography, p. 25. London: Academic Press.
TEMPLETON, D. H. (1955). Acta Cryst. 8, 842.
UEKI, T., ZALKIN, A. & TEMPLETON, D. H. (1966). Acta Cryst. 20, 836.

Absolute Measurement of Structure Factors of Si by Using X-ray Pendellösung and Interferometry Fringes

By S. TANEMURA AND N. KATO

Department of Applied Physics, Nagoya University, Nagoya, Japan

The absolute values of crystal structure factors $|F_g|$ of silicon were determined accurately for five low-order lattice planes, with probable errors of less than 0·05 %. The principle of the measurement is to take the ratio of $|F_g|$ and $|F_0|$, which are geometrically proportional to the spacings of the Pendellösung and interferometric fringes respectively. Thus, this method is not only based on a principle appropriate for a truly absolute measurement, but the difficulty in determining the proportional factors is essentially eliminated, and the experimental errors can be reduced to about 0·1 %. Some geometrical corrections, however, are required to attain an accuracy better than this. These corrections as well as the theoretical ones are discussed and the necessity of taking into account the effect of the nuclear Thomson scattering is pointed out. The consistency of the results was checked with respect to the following points; (i) $|F_g| = |F_{-g}|$, (ii) $|F_g|$ values being independent of whether the interference fringes in the direct beam or those in the Bragg-reflected beam are used, and (iii) the agreement of $|F_g|$ for different specimens. The atomic scattering factors $|f_g|$ standardized at 20°C are as follows; 111: 10·66$_0$, 220: 8·46$_0$, 333: 5·83$_9$, 440: 5·40$_4$, and 444: 4·16$_8$. A comparison is made with the values of other authors.

1. Introduction

One of the important topics in crystallography is the determination of accurate values of structure factors on an absolute scale. The methods can be classified in two categories; (i) the methods based on the kinematical theory and (ii) those based on the dynamical theory of crystal diffraction. Obviously, the former is universal but cannot be very accurate, while the latter holds the possibility of obtaining very accurate values for limited

kinds of substances. The second method is further classified into two groups, (i) the methods based on the rocking curves and (ii) those based on interference fringes due to the dynamical diffraction. Among the methods of the second group, one can use Pendellösung fringes in Laue cases (Kato & Lang, 1959; Hattori, Kuriyama, Katagawa & Kato, 1965; Yamamoto, Homma & Kato, 1968; Kato, 1969; Hart & Milne, 1969; Persson, Zielińska-Rohozińska & Gerward, 1970), Borrmann and Lehmann's fringes in Laue–Bragg–Laue cases* (Borrmann & Lehmann, 1963; Lehmann & Borrmann, 1967) and Hart & Milne's (1970) fringes for transmitted waves through two crystal slabs.

The present authors (Kato & Tanemura, 1967) proposed a method of determining the structure factors $|F_g|$ on a truly absolute basis by combining the fringes appearing in Pendellösung and interferometry experiments. The interferometer used is essentially similar to that of Bonse & Hart (1965). This paper presents the experimental atomic scattering factors, $|f_g|$, for five low-order reflexions from silicon single crystals. The probable errors from independent measurements were less than 0·05%.

In § 2, the principles for the ideal geometric conditions are described and in §§ 3 and 5, the experimental technique and some preliminary experiments are described. Since the probable errors in measuring the fringe spacings were reduced to ~0·1–0·03%, several conceivable experimental and theoretical errors larger than 0·02% are discussed in § 4. In the final section, the $|f_g|$ values obtained are compared with the results of the authors mentioned above.

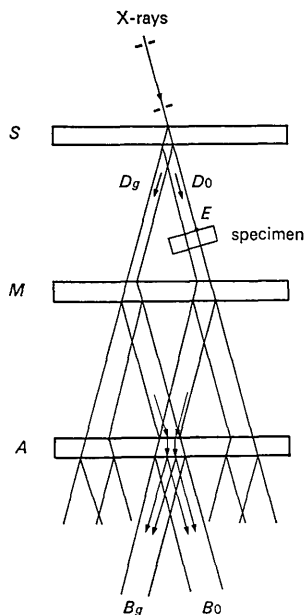* The terminology is explained in the paper of Saka, Katagawa & Kato (1971).

Fig. 1. The principle of X-ray interferometry.

2. Principles

For an ideal geometrical arrangement, the spacing A_0 of the X-ray interferometry fringes and the spacing A_g of the Pendellösung fringes are proportional to the zero and gth order structure factors, $|F_0|$ and $|F_g|$ respectively. The present method essentially determines $|F_g|/|F_0|$ by taking the ratio of A_0 and A_g, which are measurable from the interferogram and the diffraction topograph respectively.

An X-ray interferometer of the Mach–Zehnder type, developed by Bonse & Hart (1965a,b), was constructed. The interferograms used are, however, different from theirs. Those obtained by Bonse & Hart are of the traverse type, whereas the present ones are of the section type, the terminology being that used for Lang's X-ray topographs (Lang, 1957, 1959; Kato & Lang, 1959).

The interferometer is composed of three crystal plates, which are hereafter denoted by S, M and A as shown in Fig. 1. A very narrow beam is used as the incident beam. After penetrating the crystal S, both the direct and Bragg-reflected beams are broadened as in the case of the Borrmann fan. Similarly, the beam-widths are doubled and trebled after passing through the crystals M and A respectively. If we insert a wedge-shaped specimen C in the beam D_0, interference fringes appear in both the beams B_0 and B_g. Interference occurs owing to the phase difference φ_C between the two waves arriving at a point on the photographic plate. The increment of the path length of the beam D_0 in the specimen, corresponding to an increment 2π in the phase φ_C [cf. Fig. 2(a)], is given by

$$A_0^C = \lambda/|n_C - 1| = 2 \cdot \left(\frac{\pi v}{\lambda}\right)\left(\frac{mc^2}{e^2}\right)/|F_0| \qquad (1)$$

where n_C is the refractive index of the specimen for X-rays, λ the wavelength, v the volume of the unit cell, m, c and e are the physical constants having their usual meanings, and $|F_0|$, is essentially the total number of electrons contained in the unit cell.

The observed fringe spacing A_0 is given by

$$A_0 = A_0^C \Phi_0 \qquad (2)$$

where Φ_0 is a geometrical factor depending on the orientation of the entrance and exit surfaces with respect to the X-ray beam. In the particular case where the entrance surface is perpendicular to the beam, Φ_0 is cot φ, where φ is the wedge angle between the cross-section of the specimen and the plane of the incident beam.

As to the Pendellösung fringes, the diffraction topographs of the section type are used as by Hattori, Kuriyama, Katagawa & Kato (1965). As shown in Fig. 2(b), an intensity field characterized by the hyperbolic Pendellösung fringes, with the asymtotes ET and ER, appears within the specimen. The fringe spacing A_g^C along

the lattice plane, on which the apexes of the hyperbolae lie, is given by

$$A_g^C = \left(\frac{1}{\cos \theta_B}\right)\left(\frac{\pi v}{\lambda}\right)\left(\frac{mc^2}{e^2}\right)/|F_g| \qquad (3)$$

including the effect of polarization of the X-rays, where θ_B is the Bragg angle. Pendellösung fringes in a section pattern are an oblique projection of the fringes appearing on the exit surface. Therefore, the observed fringe spacing A_g along the bisector of the wedge pattern is connected with the fringe spacing A_g^C by a geometrical factor Φ_g:

$$A_g = A_g^C \Phi_g . \qquad (4)$$

Examples of section topographs are shown in Fig. 3.

When the beam paths are identical for both the interferometer and Pendellösung experiments, the factors Φ_0 and Φ_g are related by $\Phi_g = A\Phi_0$, where A is a geometrical factor given by

$$A = \frac{\cos(\omega/2)}{\sqrt{\cos \omega}} \times \sqrt{1 - \tan^2 \alpha \tan^2 \theta_B} \qquad (5)$$

(see Appendix A). In this expression, ω is the wedge angle of the section topograph and α is the angle shown in Fig. 7, which indicates the deviation from the condition of symmetrical Laue geometry with respect to the exit surface. By combining equations (1), (2), (3) and (4), the ratio $|F_g|/|F_0|$ is given by

$$|F_g|/|F_0| = \left(\frac{1}{2 \cos \theta_B}\right)\left(\frac{A_0}{A_g}\right) . A . \qquad (6)$$

The structure factor $|F_g|$ can be determined in this way on the scale of $|F_0|$ by obtaining the fringe spacings A_0 and A_g and the wedge angle ω. In contrast to the case of Hattori, Kuriyama, Katagawa & Kato (1965), the final result is not sensitive to the angle ω since it appears only through the cosine in equation (5).[*]

In practice, interference fringes of the moiré type appear in B_0 and B_g beams in Fig. 1 even if no specimen crystal is inserted in D_0. These fringes are called the intrinsic fringes and are shown in Fig. 4(a). They are due to the lattice distortion and faults in the interferometer crystal. The real phase difference in the experiment of interferometry is, therefore, given by

$$\varphi_r = \varphi_c + \varphi_i \qquad (7)$$

instead of φ_c, where the additional phase φ_i is the intrinsic phase difference between two optical paths divided by the splitter S. An example of the fringes with a wedge-shaped specimen is shown in Fig. 4(b).

In the simplest case, in which the phases are linear with respect to the beam height along which the fringe spacings are measured, the true spacing A_0 is given by

$$\frac{1}{A_0} = \frac{1}{A_r} - \frac{1}{A_i} \qquad (8)$$

where A_r and A_i are observed spacings in the experiments respectively with and without the specimen. The assumed linearity was examined experimentally, and the more refined treatments will be discussed later.

3. Experimental

3.1 Specimens

A single crystal was supplied from a commercial source. It was grown along the [111] axis. The specimens were prepared in a form of 20° wedges by polishing, with the use of a metal jig. Three types of specimens with different orientations were prepared. In type I, one of the wedge surfaces was (111), i.e. perpendicular to the growth direction; in type II, the wedge surface was (211), parallel to the growth direction; in type III, the wedge surface was perpendicular to (111) which
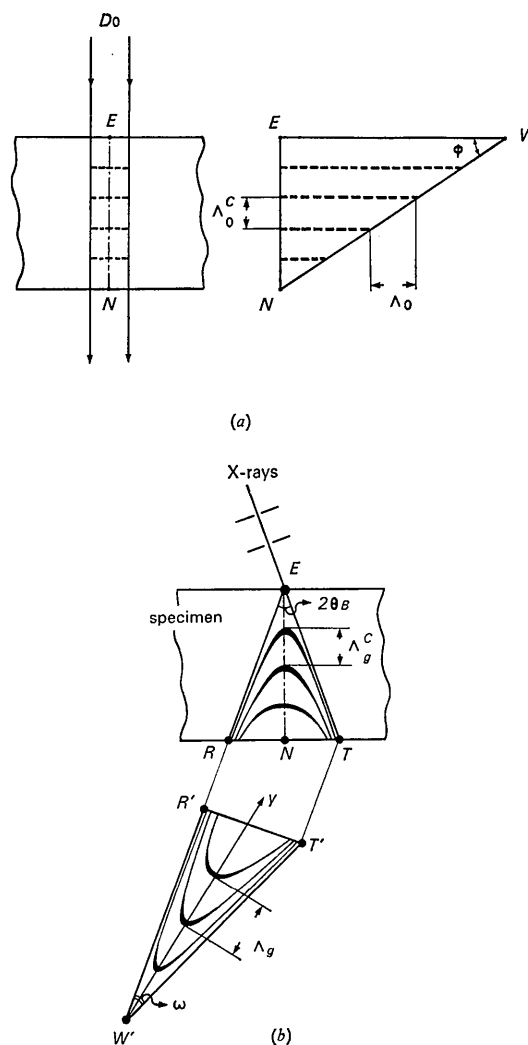

Fig. 2. (a) The relation between the observed spacing A_0 and the spacing A_0^C which is virtual in the crystal. (b) The relation between Pendellösung fringes in the crystal and in the section topograph.

---

[*] The factor $(1 - \tan^2 \alpha \tan^2 \theta_B)^{1/2}$ is regarded as a correction term.

is oblique to the growth direction. After polishing, surface strains were etched off using hydrofluoric acid.

3.2 Interferometer

The Bonse–Hart interferometer was made from a rod of Si single crystal, which also was grown along the [111] axis. The lattice plane used for Bragg reflexion was (220) in S, M and A crystal plates in Fig. 1. The thickness of each plate was 2·10 mm. The distances between S and M, and between M and A were 16·5 mm. Ag $K\alpha_1$ radiation was used throughout the present experiment. Under these conditions, the attenuation index $\mu_0 t$ for a single plate was about 1·6. The width of the coherent wave front in both B_0 and B_g beams was about 1·8 mm.

3.3 Spectrometer

A new type of double crystal spectrometer was designed, in which two crystal stages, A and B, were arranged vertically. The stage A was removable from the X-ray path by an upward traverse, and the stage B was movable by a horizontal traverse. Each stage was rotated precisely about a vertical axis. The incident X-rays were collimated by two vertical slits so as to pass through the rotation axis of the specimen, the parallelism being checked to an accuracy of 10′ of arc.

The interferometer crystal was suspended from the stage A with four hooks, the lattice plane of the interferometer being made vertical by adjusting the lengths of the hooks.* The specimen crystal was mounted on a goniometer head attached to the stage B. Again, the lattice plane was made vertical. For the present experiment, it was also necessary for the entrance surface to coincide with the plane determined by the rotation axis and the horizontal traverse direction of the stage B. Actually, by the use of an optical microscope, it was confirmed that the angle between the entrance surface and the vertical axis was less than 5′, and the horizontal distance between the rotation axis and the entrance surface was less than 10μ. The angle between the entrance surface and the traverse direction was estimated to be less than about 1°. These conditions were kept before and after both the rotation and the small horizontal traverse of the stage B necessary for taking Pendellösung and interferometry fringes (see § 3·4).

The holder of the photographic plate was put on the counter arm. This arm was rotated about the same vertical axis as that for the specimen so that the plate could be set perpendicular to the Bragg-reflected beam within the accuracy of machining. The relative angular position of the counter arm was read to an accuracy of 1′ of arc.

The apparatus including the X-ray source was set up in a room in which the temperature was controlled by an electronic device to within ±2°C. A series of Pendellösung and interferometry experiments with and

* This condition was attained when the narrowest rocking curve was obtained.

without the specimen was performed at the same temperature. Different series of experiments, however, were performed between 20 and 30°C.

3.4 Experimental procedure

The first step of the experiment was to take Pendellösung fringes. In this experiment, the interferometer crystal was first lifted above the X-ray beam. Next, interferometry fringes with the specimen were recorded. Beforehand, the specimen had been rotated through the Bragg angle θ_B and displaced by the half-width of the beam D_0 on the entrance surface ($=310\mu$). The accuracy of the rotation was about 1′ and the displacement was measurable down to 10μ. By this procedure, the requirement, $\Phi_g = A\Phi_0$, mentioned in connexion with equation (5) was fulfilled with sufficient accuracy. After changing the geometry of the specimen, the interferometer crystal was brought down in a position and orientation, such that the Bragg condition was satisfied. The counter arm, on which the plate holder was fixed, was turned to make the plate nearly perpendicular to either one of the beams, B_0 and B_g.

Finally, the specimen crystal was removed from the beam D_0, and the intrinsic interferometry fringes were recorded. In some cases, the specimen was brought back to the original position and the taking of interferometry and intrinsic fringes repeated.

The methods for obtaining the spacing A_g of the Pendellösung fringes and the wedge angle ω of the section topograph were the same as those described by Hattori, Kuriyama, Katagawa & Kato (1965). The fringe spacing was measured along the bisector (y) of the wedge pattern [Fig. 2(b)]. In the case of the interferometry and intrinsic fringes, the spacings were measured along the central line of each topograph. In determining the spacings of the three kinds of fringes, care was taken to use the fringes corresponding to the same region of the beams. Because of the principles of the present method, it was not necessary to calibrate the distance measurements on an absolute scale.

4. Preliminary experiments

(1) As mentioned in the last section, we need to rotate and traverse the specimen before taking interferometer fringes in order to satisfy the condition $\Phi_g = A\Phi_0$. If, however, the rotation axis does not lie on the entrance surface, the specimen may be displaced in an undesirable way. The rotation angle may also include some errors. When the wedge of the specimen is not accurately shaped, the ideal geometric conditions may not be fulfilled. In order to check the errors owing to these faults in the geometry, the following experiments were carried out.
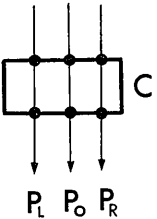
(i) The change in the fringe spacings A_r was examined over a traverse range of 2 mm (see Table 1a).

(ii) The change of A_r was examined over a rotation angle of 1° [see Table 1(b)].
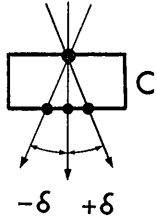
Table 1. *The fringe spacings*

(a) Different entrance points

Position	Λ_r (mm)	
P_0	0.1 3 4 6 1	
P_R	0.1 3 4 7 1	
P_L	0.1 3 4 6 1	
P_0	0.1 3 4 7 2	

(b) Different penetration

Angle δ	Λ_r (mm)	
$-30'$	0.1 3 4 5 4	
$-20'$	0.1 3 4 6 1	
$-10'$	0.1 3 4 5 4	
$0'$	0.1 3 4 4 7	
$+10'$	0.1 3 4 5 7	
$+20'$	0.1 3 4 4 6	
$+30'$	0.1 3 4 4 6	

No systematic changes were detected. The probable errors in the data listed in Table 1(a) and (b) were 0·030 and 0·029% respectively. The probable error in each of the data arising from the measurement of the distances was about 0·02%.* Therefore, the errors caused by misadjustment and the unevenness of the specimen were neglected.

(2) It takes more than 50 hours to obtain a set of three interferograms. Therefore, whether the specimen and interferometer crystals moved must be investigated. For this purpose, interferometry fringes with and without specimen were taken alternately over a period of 20 days and their spacings were compared. The results are listed in Table 2(a) and (b). The probable errors in these data were about 0·034 and 0·14% respectively. Since the means of the probable errors in Λ_r and Λ_i in individual experiments were 0·015 and 0·13% respectively,† it was again concluded that the crystal movement was negligibly small under the present experimental conditions.

---

* According to Fisher's F-test (Lehmann, 1959), the b variance σ_b^2 among the set of data is about 1/30 of the w variance σ_w^2 within the individual data.

† For the spacing Λ_r, $\sigma_b^2 \sim (1/30)\sigma_w^2$ and σ_b^2 is negligible for the spacing Λ_i.

Table 2. *Aging tests*

(a) Λ_r

Plate No.	Days	Λ_r (mm)
62	—	0·13493
64	3	0·13493
66	6	0·13489
68	13	0·13504
70	20	0·13483

(b) Λ_i

Plate No.	Days	Λ_i (mm)
63	—	0·4439
67	5	0·4453
69	12	0·4454
71	20	0·4433

(3) According to the principles of interferometry, we may expect the spacing Λ_0 to be independent of whether the beam B_0 or B_g is used. It seems worth while, therefore, to examine this experimentally. Table 3 shows the comparison of the fringe spacings based on the B_0 and B_g beams. The difference was 0·12% without the correction for vertical divergence and was reduced to 0·03% by use of the proper correction.*

Table 3. *The comparison between Λ_0 values obtained from the beams B_0 and B_g*

Beam	Λ_0 (mm)
B_0	$0.1742_0 \pm 0.0001_0$
B_g	$0.1743_1 \pm 0.0000_7$

This result confirmed the validity of both the principle of the experiment and the correction for vertical divergence. Thus, in principle, both the B_0 and B_g beams can be used for determining Λ_0. In practice, however, it was much easier to determine the central line with the B_g beam by virtue of the two parallel lines, which can be interpreted as the margin enhancement produced by the direct beam in the section pattern of the M crystal. These parallel lines must be symmetrical with respect to the central line of the B_g beam. For this reason, the B_g beam was used in the following experiments.

5. Corrections

In this section, several corrections are discussed for possible errors which may exceed 0·02%. The first four are referred to as the experimental errors while the remainder are those pertinent to theoretical principles.

5.1 The linearity of the phases

The assumption of the linearity of φ_c is true only when the crystal wedge is ideally shaped. When the specimen surfaces were wavy, not only the spacing Λ_0 but the spacing Λ_g would have variations with the ver-

---

* The vertical correction for B_g is described in §5·3. The correction for B_0, which is different from that for B_g, can be found using similar principles.

tical height of the crystal. For most measurements of the sets of the 111 and 220 reflexions, for which A_g could be determined accurately, no appreciable variation was noticed and the fringe spacings were determined with an accuracy of about 0·03%, which was comparable to the intrinsic error in the measurement of distance. For this reason, it was concluded that the linearity of φ_C was sufficient.

Next, we discuss the procedure for determining A_0 when φ_i is not linear with the crystal height h. In general, it may be natural to take a polynomial approximation

$$\varphi_i(h) = \sum_{m=0}^{N} \alpha_m h^m . \tag{9}$$

Obviously, φ_i are πk (k: integers) at the maxima and minima of the fringes in the interference experiment. Thus, assuming the polynomial order N, we can determine the coefficients α_m and the standard deviation σ of φ_i by the method of least squares. In our experiment, it was recognized that $\sigma(N)$ decreased rather critically for a polynomial order N larger than N^*. [Incidentally, N^* was less than 4 in our experiments.] Once N^* was fixed, by virtue of equation (7), we obtained the relation

$$\varphi_C(h) \equiv \beta_0 + \beta_1 h = \varphi_r(h) - \sum_{m=0}^{N^*} \alpha_m h^m \tag{10}$$

where φ_C had already been confirmed as linear in h. By definition, $2\pi/\beta_1$ is the fringe spacing A_0. Since the values $\varphi_r(h)$ must be πl (l: integers) at the maxima and minima of the fringes, A_0 can be determined by the method of least-squares. Some numerical values of A_0 and the probable errors are shown in Table 4, as well as $\sigma(1)$ and $\sigma(N^*)$. Although the present procedure results in no significant change in A_0, the probable errors ε are improved appreciably.

5.2 The departure from the symmetrical Laue condition

Since the ideal geometrical condition was not attainable, the deviation angle α defined in Fig. 7 was estimated experimentally by using the pair of wedge angles ω and $\bar{\omega}$ of the section patterns for g and $\bar{g}$ reflexions. According to Appendix A, α is given as

$$\tan \alpha = \frac{\tan \omega - \tan \bar{\omega}}{\tan \omega + \tan \bar{\omega}} \cot \theta_B . \tag{11}$$

Since $\tan \alpha$ must be constant for each specimen, α values determined from various reflexions are averaged. The values of the correction factor $(1 - \tan^2 \theta_B \tan^2 \alpha)^{1/2}$

contained in equation (6) are listed below. The correction is negligible in other cases.

Specimen	Reflexion	Correction factor
II-1	333	0·9997
III-2	333	0·9997
III-2	444	0·9995

5.3 The vertical divergence of the X-ray beam

Since, in practice, the incident beam diverges vertically, the fringe spacings are magnified by a factor, depending on the distance (L) between the source and the entrance surface of the specimen and on the optical distance (l) between the entrance surface and the recording plate. From geometrical considerations, the experimental values of the spacings are given by

$$A_0 = (A_0)_c \frac{L_0 + l_0}{L_0} \tag{12a}$$

$$A_g = (A_g)_c \frac{L_g + l_g}{L_g} \tag{12b}$$

where the suffix c denotes the spacing in the case of an ideally parallel beam and suffixes 0 and g refer to the interferometry fringes and Pendellösung fringes respectively. In deriving equation (12b), it is assumed that the optical paths are identical for the interferometry experiments, both with and without the specimen. The correction factor V to A_0/A_g, therefore, is given by

$$V = \left(\frac{L_0}{L_0 + l_0}\right) \Big/ \left(\frac{L_g}{L_g + l_g}\right). \tag{13}$$

Throughout the experiment L_0 and L_g were about 440 mm. Since L_0 is very close to L_g, the absolute accuracy is not important in view of the functional form of equation (13). The distances, l_0 and l_g are about 50 mm, the exact value varying between individual experiments.

(a) The estimation of l_g

In the ideal case of the Pendellösung experiment, the photographic plate must be set perpendicular to the diffracted beam EG_1 on the counter arm* (see Fig. 5) and the rotation axis C of the counter arm is to be identical with the rotation axis E of the specimen. As a first trial, therefore, l_g was estimated as $l.\cot 2\theta_B$, with $l = G_1 D$, measured on the photographic plate. The

---

* Precisely speaking, G_1 is the edge of the section topograph corresponding to the entrance point E.

Table 4. *The linearity correction in* A_0

No.	N^*	$\sigma(1)$ ($\times 10^{-3}$)	$\sigma(N^*)$ ($\times 10^{-4}$)	Uncorrected (eq. 8)		Corrected (eq. 10)	
				A_0 (mm)	$\frac{\varepsilon}{A_0}$ ($\times 10^{-4}$)	A_0 (mm)	$\frac{\varepsilon}{A_0}$ ($\times 10^{-4}$)
1	3	1·0	4·2	0·19667	4·8	0·19665	2·9
2	3	2·2	6·9	0·19653	7·1	0·19659	4·3
3	2	1·6	5·2	0·17446	4·3	0·17447	2·8
4	2	0·6	3·3	0·17423	2·3	0·17416	2·7

direct beam D was recorded for low order reflexions. Then, l_g was expected to be constant. Unfortunately, the variation in l_g shown in Fig. 6 was noticed. Two causes are conceivable for this variation: (i) The rotation axis C does not coincide with the axis E, and (ii) the plate holder is not exactly perpendicular to the beam EG_1. By taking account of these factors, the radius of the circles G_1 round the axis C is approximately given as

$$R \equiv CG_1 = l_g + a \cdot \cos(2\theta_B - \psi) \qquad (14)$$

where the distance a and the angle ψ are shown in Fig. 5. The distance l_g is now estimated as

$$l_g = l \cdot (\cot 2\theta_B + \delta) \qquad (15)$$

where δ is the deviation angle due to the error in machining the plate holder (see Fig. 5). By definition, the radius R must now be constant instead of $l.\cot 2\theta_B$. The angle δ must also be constant throughout the experiments.

With a trial value of δ, the corrected distance l_g given by equation (15) was again plotted against $2\theta_B$. According to equation (14), the functional form $l_g(2\theta_B)$ must equal $\{R - a \cdot \cos(2\theta_B - \psi)\}$. In practice the experimental curves $l_g(2\theta_B)$ were well represented by this form with $\psi = 90°$. By this procedure, R and a could be determined for any trial value of δ. Once these were obtained, the values of l_g for higher order reflexions were determined by means of the extrapolation of the curve $l_g(2\theta_B)$. The choice of a reasonable value of δ will be mentioned later.

(b) The estimation of the distance l_0

In the interferometry experiments, as shown in Fig. 5(b), the counter arm was turned about the axis C and was set at an angle 2θ. The distance $l_0 = EA + AG_2$ can be given as

$$l_0 = l_g(2\theta) \cdot \{1 + \sigma(2\theta)\}. \qquad (16)$$

Here, the distance $l_g(2\theta)$ is estimated by interpolation of the curve $l_g(2\theta_B)$ mentioned above. The correction term $\sigma \simeq 2 \tan \theta_{220} \cdot (\theta - \theta_{220})$ amounts to 4×10^{-3} in the present case. The angle 2θ is measured directly to an accuracy better than 10^{-2}, which is enough for determining $l_g(2\theta)$ and $\sigma(2\theta)$.

Because $L_0 \simeq L_g$, the accuracy of V is essentially determined by the error in $[l_g(2\theta_B) - l_g(2\theta)]$, which is estimated to be ± 0.1 mm. Thus, finally, the accuracy of V is estimated to be about $\pm 2 \times 10^{-4}$.

(c) The estimation of the deviation angle δ

In our experiments, a systematic discrepancy between non-corrected values of $|F_g|$ and $|F_{-g}|$ was recognized for every reflexion. This discrepancy had been anticipated from the systematic variation of the distance l_g, mentioned in the above section. In fact, we could minimize the discrepancy by selecting an optimum value of the deviation angle δ. In the following, the root S of a variance defined by $\frac{1}{5}\sum_g \{\langle|F_{+g}|\rangle - \langle|F_{-g}|\rangle\}^2$ is listed for each trial value of δ, where $\langle|F_{\pm g}|\rangle$ are the mean structure factors corrected by the factor V.

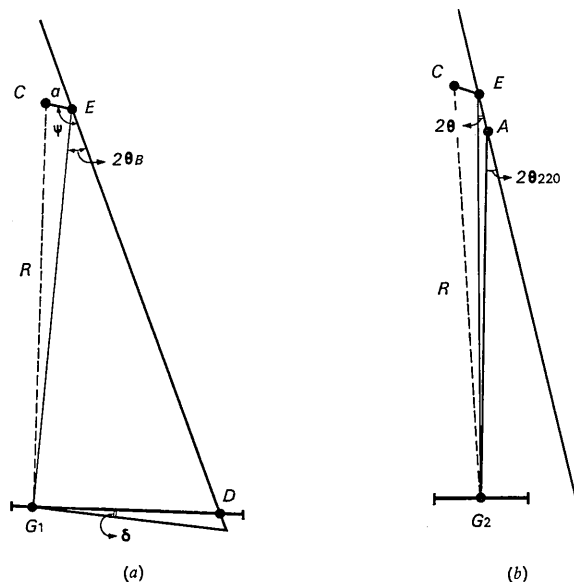| δ	a(mm)	$S \times 10^4$
0°	1·69	121
40′	0·95	43
1°00′	0·57	9
1°20′	0·31	45
non-corrected value		57

Fig. 5. (a) The geometry for determining l_g ($= \overline{EG_1}$). (b) The geometry for determining l_0 ($= \overline{EA} + \overline{AG_2}$). E: The axis of crystal rotation. C: The axis of the counter arm. D: The direct image of the incident beam. G_1: The image of the Bragg reflected beam in the Pendellösung experiment. G_2: The image of the B_g beam in the interferometry experiment. A: The intersection of the direct beam and the central line of the M crystal. Both G_1 and G_2 lie on the circle of radius R.

Table 5. *The correction factor W due to temperature effects*

	$\Theta_M = 543°K$		$\Theta_M = 538°K$	
	$\Delta T = 5°$	$\Delta T = 10°$	$\Delta T = 5°$	$\Delta T = 10°$
111	0.16×10^{-3}	0.32×10^{-3}	0.17×10^{-3}	0.33×10^{-3}
220	0·43	0·86	0·44	0·88
333	1·45	2·91	1·48	2·97
440	1·72	3·44	1·76	3·52
444	2·58	5·17	2·68	5·28

Plate 3

220

440
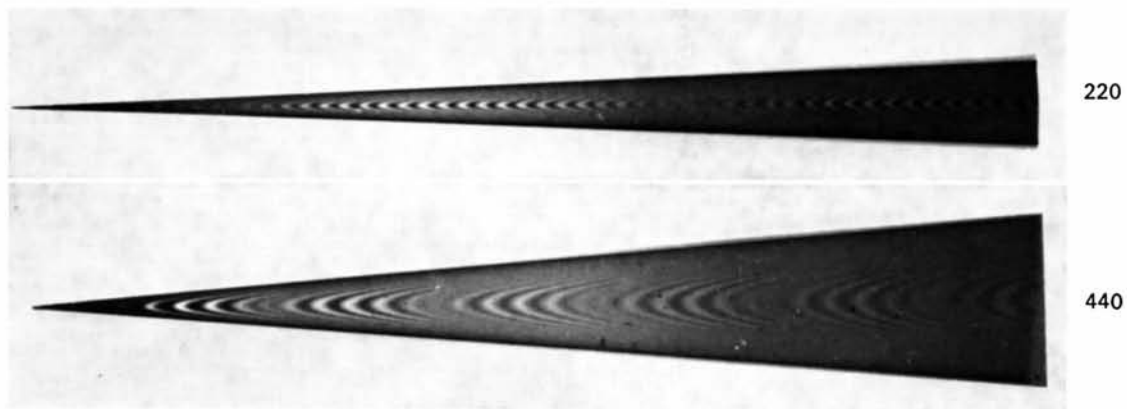
Fig. 3. The section topographs of the 220 and 440 reflexions.
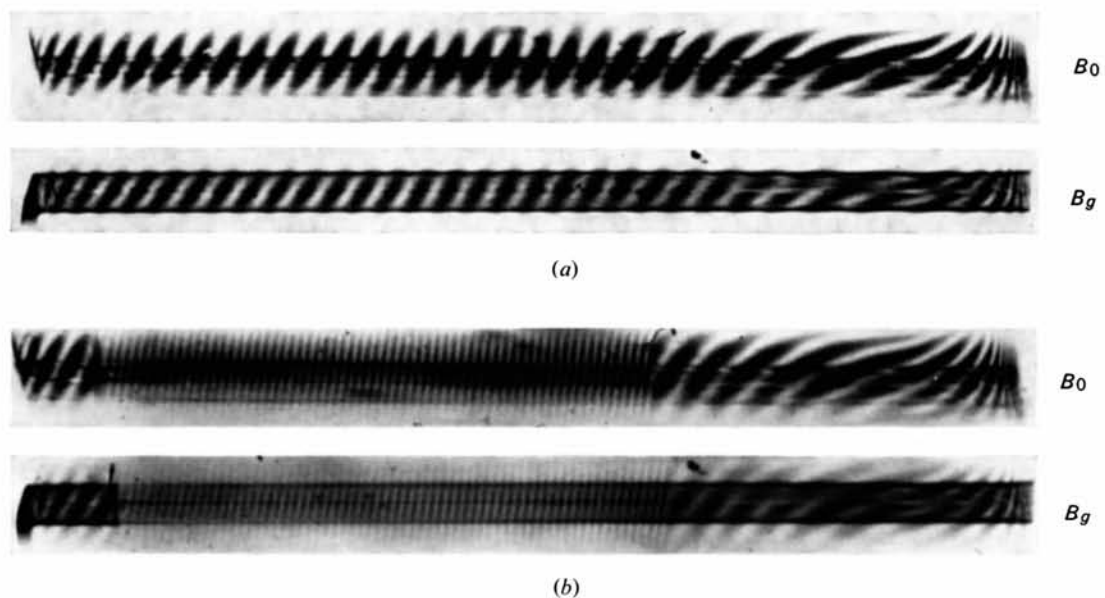

B_0

B_g

(a)

B_0

B_g

(b)

Fig. 4. Interferometry fringes; (a) without and (b) with a wedge shaped specimen.

Here, the figures in the column under a are determined according to the procedures mentioned in § 5.3(a). From this list, the deviation angle $\delta = 1°$ and the deviation distance $a = 0.57$ mm were chosen as the best. These figures are reasonable from the point of view of the mechanical accuracy of the apparatus used. With these values, $|V-1|$ amounts to about 2×10^{-4} for the set of 111 reflexions and about 7×10^{-4} for the 444 reflexions.

5.4 The effects of temperature

Because the mean temperatures in the individual experiments were different as explained in § 3.3, corrections are required to the observed values $|F_g|/|F_0|$. It is obvious that the effect of thermal expansion is cancelled out in $|F_g|/|F_0|$.

An important correction is required owing to the effect of the Debye–Waller factor e^{-M} in $|F_g|$, where M is given by the standard formula (James, 1962),

$$M(T) = \frac{6h^2}{mk\Theta_M}\left\{\frac{1}{4} + \frac{\Phi(x)}{x}\right\} \cdot \left(\frac{\sin\theta}{\lambda}\right)^2. \quad (17)$$

In order to take a significant average over the different experiments, we need to multiply by the correction factor

$$W = \exp[M(T) - M(293)]. \quad (18)$$

Here, for convenience, the whole data are reduced to the values at 293 °K. An ambiguity may arise about the Debye temperature Θ_M. Actually, however, the correction factors W calculated on the basis of $\Theta_M = 543$ °K (Batterman & Chipman, 1962) and $\Theta_M = 538$ °K (Hat-

tori, Kuriyama & Kato, 1965) are close enough to each other, with an accuracy of 10^{-4} as shown in Table 5. The linearity of the correction is also confirmed within this temperature range. Here, it seems worth mentioning that the temperature dependence of the Debye function was calculated with the required accuracy, although the temperature dependence of the Debye temperature was neglected.

In the following table, the ratios of the standard deviation σ and the structure factor $|F_g|$ are listed for each reflexion* in parts per thousand.

	Non-corrected	Corrected
111	1·52	1·51
220	0·62	0·51
333	2·25	2·00
440	1·61	1·09
444	0·02	0·35

The corrected values of $\sigma/|F_g|$ are smaller than the non-corrected values except for 444, for which the statistical treatment is meaningless since the number N of the experiments was only two. For this reason, the temper-

* Non-corrected: $\sigma^2 = \dfrac{1}{N-1}\left[\displaystyle\sum_{i=1}^{N}\{|F_g|_i - \langle|F_g|_i\rangle\}^2\right]$

Corrected: $\sigma^2 = \dfrac{1}{N-1}\left[\displaystyle\sum_{i=1}^{N}\{W_i|F_g|_i - \langle W_i|F_g|_i\rangle\}^2\right]$

The suffix i covers the individual experiments.

Table 6. $|f_g|$ values

(a) hhh series.

Specimen	111 g	111 −g	333 g	333 −g	444 g	444 −g
II−1	10·678	10·681				
	10·655	10·644	5·830	5·833		
	10·687	10·682				
III−1	10·646	10·630	5·825	5·843		
	10·660	10·667	5·859	5·838		
	10·667	10·674	5·834	5·822		
	10·648	10·650	5·850	5·853		
III−2	10·640	10·652	5·829			
	10·665	10·651				
			5·848	5·848		
					4·167	4·170
σ_m	0·008	0·008	0·014 ˙	0·011	0·010	0·012
σ	0·015	0·018	0·013	0·011	–	–
mean	10·661	10·659	5·839	5·840	–	–
$\bar{\sigma}$	0·005	0·006	0·005	0·005	–	–

(b) (hh0) series.

Specimen	220 g	220 −g	440 g	440 −g
I−2	8·459	8·456	5·400	5·399
	8·453	8·457	5·397	5·400
	8·463	8·466	5·413	5·409
I−3	8·462	8·462	5·403	5·401
σ_m	0·008	0·007	0·008	0·008
σ	0·004	0·005	0·007	0·006
mean	8·459	8·460	5·403	5·404
$\bar{\sigma}$	0·002	0·002	0·004	0·003

ature correction with the use of Table 5 is regarded as significant.

5.5 The effects of dispersion

The Fourier coefficient F_0 differs from $8Z$ by the dispersion correction $8(\Delta f_0' + i\Delta f_0'')$, Z being the atomic number of Si. According to Cromer (1965), $\Delta f_0' = \Delta f_0'' = 0.06$ are given for Ag $K\alpha_1$ radiation. In equation (6), therefore, the corrected value $|F_0| = 112\{1 + 4.3 \times 10^{-3}\}$ was used. Theoretically speaking, the Fourier coefficient $|F_g|$ should also be corrected for the dispersion effect. However, because the g-dependence of the correction is not certain, the uncorrected values of $|F_g|$ are listed in Tables 6 and 8.

5.6 The refractive index of air

Equation (1) assumes unity for the refractive index of air, n_a. If one takes into account the deviation 5.5×10^{-10} on the basis of the composition of standard air (American Institute of Physics Handbook, 1963), the correction factor $[1 - (n_a - 1)/(n_C - 1)]$ must be applied to $|F_0|$. The correction amounts to 5.6×10^{-4}.

5.7 Nuclear Thomson scattering (N.T.S.)

In view of the accuracy of the present experiment, the effects of N.T.S. cannot be neglected. The nuclear scattering amplitude is given by $[(Ze)^2/M_e^2]C$, where M is the mass of the Si atom and C is the polarization factor. Thus, the atomic number Z in $|F_0|$ must be replaced by $Z[1 + (M/m)Z]$. The correction amounts to 0.027% for Si. Similarly, the correction must be made to the atomic scattering factor as follows:

$$|f_g|_{ob} = |f_g| + \frac{m}{M} Z^2. \tag{19}$$

It should be noted that the correction is significant for higher order reflexions because it is independent of scattering angle except for the polarization factor C, whereas the ordinary Thomson scattering decreases with increasing scattering angle. For example, corrections of 0.03% and 0.09% are required for the 111 and 444 reflexions respectively.
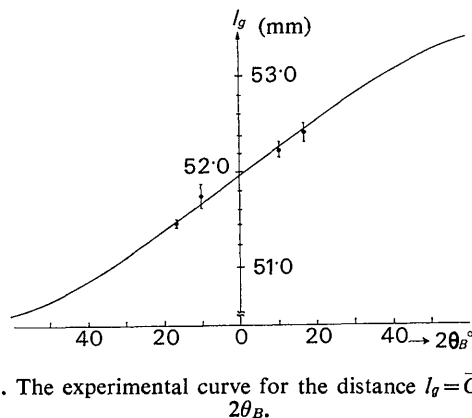

Fig. 6. The experimental curve for the distance $l_g = \overline{G_1 D} \cdot \cot 2\theta_B$.

5.8 Effects of absorption

The correction for absorption was fully discussed by Kato (1968). Since $\kappa_0 = F_0^i/F_r^g$ and $\kappa = F_g^i/F_g^r$ are less than 0.01 in the present case, the absorption effects are negligibly small.

6. Results and discussion

The atomic scattering factors $|f_g|$ are determined from the crystal structure factors $|F_g|$ and are listed in Table 6. The $|F_g|$ values are calculated by equation (6) and corrected according to the procedures described in § 5. The figures in each column are obtained from entirely independent experiments. The figures in the same row are based on the fringe spacings A_0, which are obtained from the common interferograms with and without specimens.* The standard deviations, σ_i, of the individual $|f_g|$ values are derived from those of A_0 and A_g. Their averaged values, σ_m are listed in Table 6. The σ_i values, and accordingly σ_m, are a little over-estimated because they are affected by the non-linearity of the fringe positions due to X-ray polarization (Hattori, Kuriyama & Kato, 1965) and absorption (Kato, 1968), whose effects have been disregarded in the present estimates. The dependence of σ_m on the reflexion planes is partly due to this circumstance.

At the bottom of each column, the mean value of $|f_g|$ and the standard deviations $\bar{\sigma}$ taken over a set of independent experiments are listed. Below the σ_M row, the standard deviations σ for the individual experiments are listed. By definition $\sigma = \sqrt{N} . \bar{\sigma}$ in which N is the number of experiments.†

From Table 6, one can draw the following conclusions.

(1) Since the standard deviations σ_m and σ mentioned above are comparable, most of errors included in $|f_g|$ are regarded as statistical errors in the measurement of the fringe distances.

(2) The agreement between $|f_g|$ and $|f_{-g}|$ justifies implicitly the correctness of the geometrical conditions in the present method.

(3) The values for the sets of 111 and 333 reflexions show no correlation with the growth direction of the specimen. They, as well as the values for 220 and 440, are independent of the position of the crystal rod from which the specimens are prepared. Incidentally, the result for the specimen from another source, for which the data required for the divergence correction (V) and the temperature correction (W) are unfortunately lacking, agrees also with the values listed in Table 6, within an accuracy of about 0.2%. From these results, it is reasonable to conclude that the specimens used were free from internal strains.

---

* However, the A_0 are slightly different from each other because sets of fringes in different regions must be employed.

† Roughly speaking, σ_m^2 and σ^2 correspond to the variances σ_w^2 and $\sigma_w^2 + \sigma_b^2$ respectively in Fisher's F-test (see the first footnote in §4).

Table 7. *The $|f_g|$ values of various authors**

The abbreviations, HKKK, GW and HM are explained in the text.

Index	Present	HKKK	GW†	HM	
111	10·664	10·98	10·72	8·478 (Mo)	}a
220	8·463	8·58	8·45	8·448 (Ag)	
				8·487 (Mo)	}b
333	5·843	5·86	5·90	8·494 (Ag)	
440	5·408	5·41	5·36		
444	4·172	4·22	4·18		
		(4·20)‡			

* The N.T.S. correction is omitted.
† reduced to Ag $K\alpha_1$ values.
‡ Hattori & Kato (1966).
(a) Hart & Milne (1969).
(b) Hart & Milne (1970).

In Table 7, $|f_g|$ values averaged over **g** and $\bar{g}$ reflexions, omitting the N.T.S. correction, are compared with those of other authors. The values obtained by Göttlicher & Wölfel (1959) and Göttlicher, Kuphal, Nagorsen & Wölfel (1959), (GW values), agree with the present values within an accuracy of less than 1% except $|f_{333}|$. Their method is based on intensity measurements on powder specimens. DeMarco & Weiss (1965) obtained $|f_g|$ values from intensity measurements on single crystals. Their values also agree with the GW values to on accuracy of better than 1% in most cases.§ Jennings (1969) repeated the same experiment for 111 reflexions, but his value seems to be too large.

The values of Hattori, Kuriyama, Katagawa & Kato (HKKK) (1965) based on the ordinary Pendellösung method are systematically larger than the present ones, the discrepancy being predominant in lower order reflexions. In their experiment, the geometrical factor $\Phi_g = \sqrt{\cos \omega}/\sin \omega/2$ is determined directly by measuring the angle ω of reflexion topographs. Since the tip of the wedge-shaped topograph has strong contrast, the wedge angle is apt to be measured as too small. In addition, the $|f_g|$ values of lower order reflexions are more sensitive to errors in ω. As described in connexion with equations (5) and (6), the present values are free from this cause of error.

Hart & Milne (HM) (1969) obtained values for $|f_{220}|$ by the ordinary Pendellösung method. More recently, they have measured $|f_g|$ by a different method which is based on the interference of the transmitted waves through two crystal slabs (Hart & Milne, 1970). According to their statement, the Ag values of 1970 may include some experimental errors. If one assumes Cromer's (1965) values $\Delta f_0' = 0.06$ (Ag) and 0·09 (Mo) as the dispersion correction, the mean of their three reliable values scaled on Ag values amounts to 8·454. Bearing the difference of the methods in mind, the agreement with the present results to within 0·12% is

§ Since the dispersion and temperature corrections are not clear in their data, their values are not included in Table 7.

significant in the sense that fringe methods based on the dynamical diffraction phenomena are very reliable.

The theoretical calculations of the electron distributions in free atoms (Clementi, 1965) and in crystals (Jaros & Vinsome, 1969, 1970; Stukel & Euwema, 1970) are reported. Also, the method of analysing the data of the structure factors (Dawson, 1967a, b, c; McConnell & Sanger, 1970) is presented. The theoretical values of Debye–Waller factors, the dispersion corrections and the electron distribution itself, however, do not seem accurate enough to compare the theories and the experiment. For this reason we only present the experimental values of $|f_g|$ in Table 8.

Table 8. *The final results for the atomic scattering factors of* Si *at* 20°C

Indices	$|f|$	Max. deviation	Prob. error
111	10·66$_0$	0·26%	0·02%
220	8·46$_0$	0·08	0·01
333	5·83$_9$	0·34	0·04
440	5·40$_4$	0·17	0·03
444	4·16$_8$	0·03	—

In these values, the correction for the nuclear Thomson scattering is taken into account according to equation (19). They are scaled to the values at 20°C. The dispersion correction in $|f_g|$ itself is not taken into account although this correction is included in $|F_0|$. If the accurate value of the dispersion correction $\Delta f'$ is obtained in future, the above results must be revised according to the procedures described in § 5.5.
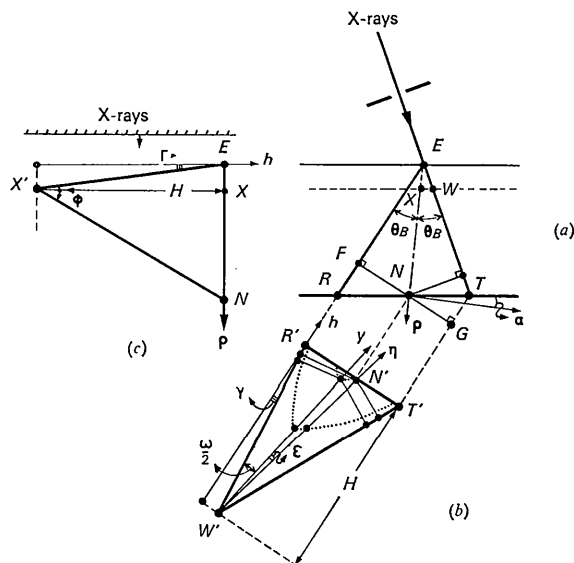

Fig. 7. (a) The horizontal section at a height H. (b) The section topograph of the Pendellösung experiment; the vertical view. (c) The vertical section of the crystal through the lattice plane EN. The broken line in (a) shows the edge of of the wedge specimen. The meanings of h, y, η, and ϱ are described in the text.

The authors acknowledge Dr I. Yoshimura for his discussion on the problems of errors. They thank also Mr Miyazaki for his help in measuring fringe spacings.

APPENDIX A

The ratio of the geometrical factor, $A = \Phi_g/\Phi_0$

Fig. 7, which is to be referred to in the following discussion, is drawn for the crystal under the conditions of the Pendellösung experiments. In the interferometry experiments, the crystal is rotated so that the lattice plane (EN) coincides with the incident beam ET. The vertical view (c) can be commonly used for both the experiments. In the interferometry experiments, the geometrical factor Φ_0 is written as

$$\Phi_0 \equiv \frac{A_0}{A_0^c} = \frac{\Delta h}{\Delta \varrho} \qquad (A1)$$

where h and ϱ are the distances along the vertical and horizontal directions in the net plane, and Δ indicates the increment corresponding to a single fringe spacing.

In the Pendellösung experiments the bisector y of the section topograph, on which the fringe spacing $A_g(=\Delta y)$ is measured experimentally, does not generally coincide with the projection line (η) of the intersection of the lattice plane and the the exit surface.* The geometrical factor Φ_g is then written in the form

$$\Phi_g \equiv \frac{A_g}{A_g^c} = \frac{\Delta y}{\Delta \eta} \frac{\Delta \eta}{\Delta h} \frac{\Delta h}{\Delta \varrho} . \qquad (A2)$$

Owing to the hyperbolic form of Pendellösung fringes, the distances y and η are connected by

$$\eta^2 \sin \left(\frac{\omega}{2} + \varepsilon\right) \sin \left(\frac{\omega}{2} - \varepsilon\right) = y^2 \sin^2 \frac{\omega}{2}$$

which gives us the relation

$$\frac{\Delta y}{\Delta \eta} = \frac{1}{\sin \frac{\omega}{2}} \sqrt{\sin \left(\frac{\omega}{2} + \varepsilon\right) \sin \left(\frac{\omega}{2} - \varepsilon\right)} \qquad (A3)$$

where ε is the angle between the directions, y and η, and the angle ω is the wedge angle of the topograph. In addition, we know that

$$\frac{\Delta \eta}{\Delta h} = \frac{1}{\cos \left(\frac{\omega}{2} + \varepsilon - \gamma\right)} \qquad (A4)$$

where γ is the inclination angle between the vertical direction and the edge $W'R'$ in the section topograph

---

* This was first pointed out by T. Katagawa in our laboratory.

corresponding to the entrance surface.† Combining the equations $(A1)$ to $(A4)$, we obtain

$$A = \frac{\Phi_g}{\Phi_0} = \frac{\sqrt{\sin \left(\frac{\omega}{2} + \varepsilon\right) \sin \left(\frac{\omega}{2} - \varepsilon\right)}}{\sin \frac{\omega}{2} \cos \left(\frac{\omega}{2} + \varepsilon - \gamma\right)} . \qquad (A5a)$$

Now, we shall rewrite this in such a way as to eliminate the angle ε, which is difficult to determine experimentally. For convenience, we shall introduce

$$E = \tan \left(\frac{\omega}{2} + \varepsilon\right) . \qquad (A6)$$

Then, we have

$$\sin \left(\frac{\omega}{2} + \varepsilon\right) = E/\sqrt{1 + E^2}$$

$$\cos \left(\frac{\omega}{2} + \varepsilon\right) = 1/\sqrt{1 + E^2}$$

$$\sin \left(\frac{\omega}{2} - \varepsilon\right) = (\sin \omega - E \cos \omega)/\sqrt{1 + E^2}$$

$$\cos \left(\frac{\omega}{2} + \varepsilon - \gamma\right) = (\cos \gamma + E \sin \gamma)/\sqrt{1 + E^2}$$

and, from these,

$$A = \frac{1}{\sin \left(\frac{\omega}{2}\right)} \sqrt{\frac{E (\sin \omega - E \cos \omega)}{(\cos \gamma + E \sin \gamma)^2}} . \qquad (A5b)$$

In Fig. 7(a) and (b)

$$R'N' \equiv \eta \sin \left(\frac{\omega}{2} + \varepsilon\right)/\cos \gamma = \varrho \sin \theta_B \equiv FN$$

$$T'N' \equiv \eta \sin \left(\frac{\omega}{2} - \varepsilon\right)/\cos (\omega - \gamma) = B\varrho \sin \theta_B \equiv GN$$

where

$$B = \frac{\cos (\theta_B + \alpha)}{\cos (\theta_B - \alpha)} .$$

By taking the ratio $R'N'/T'N'$, it is seen that

$$E = (\sin \omega \cos \gamma)/[\cos \omega \cos \gamma + B \cos (\omega - \gamma)] .$$

Substituting this into equation $(A5b)$, we obtain

$$A = \frac{\cos \left(\frac{\omega}{2}\right)}{\sqrt{\cos \omega}} \sqrt{\frac{4B}{(1 + B)^2}} \sqrt{\frac{\cos \omega}{\cos (\omega - \gamma) \cos \gamma}} \qquad (A5c)$$

where the second factor can be written in the convenient form

$$\sqrt{\frac{4B}{(1 + B)^2}} = \sqrt{1 - \tan^2 \theta_B \tan^2 \alpha} . \qquad (A7)$$

---

† For generality, we shall treat the case $\gamma \neq 0$.

In the present experiments, the angle γ can be measured directly from the angle between the edge $R'W'$ and the direct image of the direct beam, for low order reflexions. For higher order reflexions, the angle γ is estimated by

$$\tan \gamma = \frac{2 \sin \theta_B}{1+\tan \theta_B \tan \alpha} \tan \Gamma, \qquad (A8)$$

where Γ is the inclination angle between the entrance surface and the vertical plane. In all cases, Γ was confirmed experimentally to be less than 5' (cf. § 3·3). The third factor in equation $(A5c)$, therefore, is estimated to be less than 0.6×10^{-5} for 111 and 1.2×10^{-4} for 444. For this reason, this factor is omitted in equation (5).

Finally, $\tan \alpha$ in equation $(A7)$ is written in a more practical form by using a pair of wedge angles ω and $\bar{\omega}$ for g and $\bar{g}$ reflexions. Since the factor is regarded as a correction and the angle γ is small in our experiments, the entrance surface, and consequently the edge $R'W'$, are assumed to be vertical. From Fig. 7(a) and (b), we can see that

$$h \tan \omega = \varrho \sin \theta_B \cdot \{1+B\} \,.$$

For reverse reflexion, using $-\alpha$ instead of α in the factor B, we have

$$h \tan \bar{\omega} = \varrho \sin \theta_B \cdot \left\{1+ \frac{1}{B}\right\}.$$

By taking the ratio of the above two, we obtain equation (11). Since ω and $\bar{\omega}$ are obtained from a pair of the topographs of g and $\bar{g}$ reflexions, $\tan \alpha$ is determined experimentally.

References

American Institute of Physics Handbook (1963). Chap. 2, p. 134. New York: McGraw-Hill.
Batterman, B. W. & Chipman, D. R. (1962). Phys. Rev. 127, 690.
Bonse, U. & Hart, M. (1965a). Appl. Phys. Letters. 6, 155.
Bonse, U. & Hart, M. (1965b). Z. Phys. 188, 154.

Borrmann, G. & Lehmann, K. (1963). Crystallography and Crystal Perfection. p. 101. London: Academic Press.
Clementi, E. (1965). I.B.M. J. Res. Develop. 9, 2.
Cromer, D. T. (1965). Acta Cryst. 18, 17.
Dawson, B. (1967a). Proc. Roy. Soc. A298, 255.
Dawson, B. (1967b). Proc. Roy. Soc. A298, 264.
Dawson, B. (1967c). Proc. Roy. Soc. A298, 379.
De Marco, J. J. & Weiss, R. J. (1965). Phys. Rev. A137, 1869.
Göttlicher, S. & Wölfel, E. (1959). Z. Elek. Chem. 63, 891.
Göttlicher, S., Kuphal, R., Nagorsen, G. & Wölfel, E. (1959). Z. Physik. Chem. N. F. 21, 133.
Hart, M. & Milne, A. D. (1969). Acta Cryst. A25, 134.
Hart, M. & Milne, A. D. (1970). Acta Cryst. A26, 223.
Hattori, H. & Kato, N. (1966). J. Phys. Soc. Japan, 21, 1772.
Hattori, H., Kuriyama, H., Katagawa, T. & Kato, N. (1965). J. Phys. Soc. Japan, 20, 988.
Hattori, H., Kuriyama, H. & Kato, N. (1965). J. Phys. Soc. Japan, 20, 1047.
James, R. W. (1962). The Optical Principles of the Diffraction of X-rays. Chap. 5, p. 219. London: G. Bell & Sons.
Jaros, M. & Vinsome, P. K. W. (1969). J. Phys. (C) 2, 2373.
Jaros, M. & Vinsome, P. K. W. (1970). Phys. Letters, 31A, 94.
Jennings, L. D. (1969). J. Appl. Phys. 40, 5038.
Kato, N. (1968). J. Appl. Phys. 39, 2235.
Kato, N. (1969). Acta Cryst. A25, 119.
Kato, N. & Lang, A. R. (1959). Acta Cryst. 12, 787.
Kato, N. & Tanemura, S. (1967). Phys. Rev. Letts. 19, 22.
Lang, A. R. (1957). Acta Met. 5, 358.
Lang, A. R. (1959). Acta Cryst. 12, 249.
Lehmann, K. & Borrmann, G. (1967). Z. Kristallogr. 125, 234.
Lehmann, E. L. (1959). Testing Statistical Hypothesis. Chap. 7, p. 214. New York: John Wiley.
McConnell, J. F. & Sanger, P. L. (1970). Acta Cryst. A26, 83.
Persson, E., Zielińska-Rohozińska, E. & Gerward, L. (1970). Acta Cryst. A26, 514.
Saka, T., Katagawa, T. & Kato, N. (1972). Acta Cryst. A28, In the press.
Stukel, D. J. & Euwema, R. N. (1970). Phys. Rev. B1, 1635.
Yamamoto, K., Homma, S. & Kato, N. (1968). Acta Cryst. A24, 232.